Topological phase transitions, Majorana modes, and quantum simulation of the Su–Schrieffer–Heeger model with nearest-neighbor interactions

Xiang-Long Yu,[1,2] Liang Jiang,[3] Ya-Min Quan,[4] Tong Wu,[1,2] Yuanzhen Chen,[1,2] Liang-Jian Zou,[4] and Jiansheng Wu[1,2,*]

[1]*Department of Physics and Institute for Quantum Science and Engineering, Southern University of Science and Technology, Shenzhen 518055, People's Republic of China*

[2]*Shenzhen Key Laboratory of Quantum Science and Engineering, Southern University of Science and Technology, Shenzhen 518055, People's Republic of China*

[3]*Pritzker School of Molecular Engineering, University of Chicago, Chicago, Illinois 60637, USA*

[4]*Key Laboratory of Materials Physics, Institute of Solid State Physics, Chinese Academy of Sciences, P. O. Box 1129, Hefei 230031, People's Republic of China*

(Received 22 March 2019; revised manuscript received 27 November 2019; published 17 January 2020)

The Su–Schrieffer–Heeger (SSH) model is one of the simplest topological lattice models and is a promising candidate for quantum simulations of topological systems. In this study we investigate an interacting SSH model with nearest-neighbor interactions using mean field theory and an exact diagonalization method after the Jordan-Wigner transformation. We obtain a rich phase diagram with six different phases. Majorana bound states are found and confirmed by analyzing wave functions and Majorana number. In addition, we propose to use superconducting devices to construct a one-dimensional quantum circuit, where Cooper pair boxes and Josephson junctions are alternately connected in series, to theoretically simulate the interacting SSH model. This approach also provides us a toolkit to simulate correlated topological systems.

DOI: 10.1103/PhysRevB.101.045422

I. INTRODUCTION

Topological materials are at the frontier of physics research [1–7]. They have various interesting and novel properties; for example, quantum anomalous and spin Hall effects, Weyl semimetals, Majorana fermions, etc. These topological characteristics have so far been observed in several materials, such as Bi bilayer films [8], HgTe/CdTe [9] and InAs/GaSb [10] quantum wells for the quantum spin Hall effect, Cr-doped $(Bi,Sb)_2Te_3$ thin films [11] for the quantum anomalous Hall effect, the (Ta, Nb)(As, P) family of compounds [12–15] for Weyl semimetals, and the topological insulator-superconductor $Bi_2Te_3/NbSe_2$ heterostructure [16,17] for Majorana fermion states. These materials can be well understood in a single particle picture using topological band theory. However, the topological materials in the presence of strong correlation are less investigated experimentally, because the preparation of samples of related materials and observation of their properties are difficult and require high-level experimental technologies. It also makes theoretical research into strongly correlated topological systems far ahead of experimental research. Many theoretical models and novel properties remain to be verified by experiments.

Quantum simulations provide a fresh approach to this situation. A quantum physics problem may be mapped onto a mathematical model, which in turn can be straightforwardly implemented in a quantum simulator. Among various elements of quantum simulators, the Cooper-pair box (CPB), which servers as a prototypical charge qubit, is one of the most promising candidates. It uses the macroscopic quantum phenomena of superconductivity [18,19] and offers the advantage that it can be built using familiar, scalable micro-fabrication methods of conventional semiconductor fabrication. In particular, transmons [20], which are built up from a modified version of the CPB, have long experimental coherence times of $\sim$100 μs [7]. Compared with the 0 and 1 states in a classical bit, an important feature of a qubit is that any superposition of 0 and 1 states can be produced. It behaves like an artificial atom. Thus, we can use qubits to simulate condensed-matter systems and even the rich properties of various quasiparticles. Single qubits can already simulate interesting properties of condensed matters systems [6,21–32]. With improved coherence and control capability, we can use multiple qubits to simulate many-body systems [33], including simulations based on the Fermi–Hubbard model [34], the Ising model [35], anyonic fractional statistical behavior [36,37], Greenberger–Horne–Zeilinger states [38], the ground states of H_2, LiH, BeH_2 [39,40], frustrated quantum magnetism [41], the discrete time crystal [42,43], etc. Therefore, theoretical studies based on the related simulations are highly desirable to point the way toward feasible experimental schemes. In addition, such studies can also improve understanding of topological systems and predict new topological properties.

In this work, we study an interacting Su–Schrieffer–Heeger (SSH) model with nearest-neighbor interactions by mean field theory (MFT) and an exact diagonalization (ED) method. At the mean-field level, our self-consistent solution shows a rich phase diagram consisting of six different phases. The symmetry of wave functions, topological invariant, and Majorana number are also investigated to confirm the topological phase transitions. We then use superconducting qubits to construct a one-dimensional quantum circuit where CPBs and Josephson junctions (JJs) are connected alternately in series and find that the same Hamiltonian can be obtained in the quantum

*Corresponding author: wujs@sustech.edu.cn

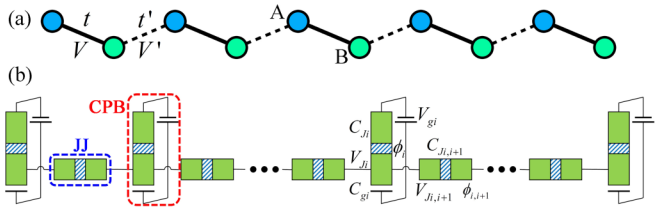

FIG. 1. (a) Schematic diagram of structure of the interacting SSH model. Blue and green circles are sites on sublattice A and sublattice B, respectively. Solid and dashed lines represent intra- and intercell interactions, respectively. (b) Schematic diagram of serial system of CPBs and JJs.

circuit as in the interacting SSH chain. The rest of this paper is organized as follows: the interacting SSH model and calculation methods are described in Sec. II; self-consistent results based on mean field theory are presented in Sec. III; finally, Sec. V is devoted to the quantum simulation of the interacting SSH model.

II. MODEL AND METHODS

A. Hamiltonian

The SSH model is one of the simplest topological lattice models; its Hamiltonian includes only nearest-neighbor hopping terms. Each unit cell consists of two sites, as illustrated in Fig. 1(a). Changing the ratio of inter- to intracell hopping parameters can induce phase transitions between topologically trivial and nontrivial states [44]. This model and its extended versions have been studied extensively over many decades [45–58]. In the extended versions, different interactions have been considered, such as Coulomb interaction, spin-orbit coupling, and superconducting pairing. Most of them focus on the spinful case. In this study we consider an interacting SSH chain of spinless fermions that includes nearest-neighbor interactions. The corresponding Hamiltonian reads

$$\begin{aligned} H = &-\sum_i \left(t c_{iA}^\dagger c_{iB} + t c_{iB}^\dagger c_{iA} + t' c_{iB}^\dagger c_{i+1,A} + t' c_{i+1,A}^\dagger c_{iB}\right) \\ &+ \sum_i \begin{bmatrix} V(2\hat{n}_{iA}-1)(2\hat{n}_{iB}-1) \\ +V'(2\hat{n}_{iB}-1)\left(2\hat{n}_{i+1,A}-1\right) \end{bmatrix} \\ &- \mu \sum_i \sum_{\alpha=A,B} c_{i\alpha}^\dagger c_{i\alpha}, \end{aligned} \tag{1}$$

where $c_{i\alpha}^\dagger$ and $c_{i\alpha}$ are fermionic creation and annihilation operators, respectively, and $\hat{n}_{i\alpha} = c_{i\alpha}^\dagger c_{i\alpha}$. The first line of Eq. (1) corresponds to the original SSH model. The second line contains nearest-neighbor interactions and chemical potential terms. The intra- and intercell interactions are expressed as V and V', respectively. We focus on the half-filling case, in which the occupation number is constrained by $\sum_\alpha \langle c_{i\alpha}^\dagger c_{i\alpha}\rangle = 1$. The mean-field method is employed to decouple four-operator terms, which are approximated by a sum of two-operator interactions.

$$\begin{aligned} \hat{n}_{i\alpha}\hat{n}_{j\beta} \approx\ & n_\alpha \hat{n}_{j\beta} + \hat{n}_{i\alpha} n_\beta - n_\alpha n_\beta + \Delta_x^* c_{j\beta} c_{i\alpha} + \Delta_x c_{i\alpha}^\dagger c_{j\beta}^\dagger \\ & - |\Delta_x|^2 - \delta_x^* c_{j\beta}^\dagger c_{i\alpha} - \delta_x c_{i\alpha}^\dagger c_{j\beta} + |\delta_x|^2, \end{aligned} \tag{2}$$

where the index $x = in$ or out corresponds to the intra- or intercell interaction, respectively, and the site-independent parameters are defined as $n_\alpha = \langle \hat{n}_{i\alpha}\rangle$, $\Delta_{\text{in}} = \langle c_{iB} c_{iA}\rangle$, $\Delta_{\text{out}} = \langle c_{iB} c_{i+1,A}\rangle$, $\delta_{\text{in}} = \langle c_{iB}^\dagger c_{iA}\rangle$, $\delta_{\text{out}} = \langle c_{iB}^\dagger c_{i+1,A}\rangle$. A finite Δ_x indicates a superconducting correlation produced by nearest-neighbor interactions. After the Fourier transformation $c_i = \frac{1}{\sqrt{N}} \sum_k c_k e^{ikr_i}$, the Hamiltonian can be written in the Nambu representation ($c_{kA}^\dagger \quad c_{kB}^\dagger \quad c_{-kA} \quad c_{-kB}$). Upon diagonalization, the corresponding eigenvalues and eigenvectors can be obtained. All order parameters are calculated self-consistently.

B. Topological invariant

To calculate the topological invariant of the mean-field Hamiltonian where there exist superconducting pairing terms, we first transform the Hamiltonian matrix into a block off-diagonal form. The unitary transformation

$$U = \begin{pmatrix} 1 & 0 & 0 & 0 \\ 0 & 0 & 1 & 0 \\ 0 & 1 & 0 & 0 \\ 0 & 0 & 0 & 1 \end{pmatrix} \tag{3}$$

is introduced to transform the Hamiltonian matrix:

$$U h(k) U^\dagger = \begin{pmatrix} 0 & F \\ F^\dagger & 0 \end{pmatrix} \tag{4}$$

with

$$F = \begin{pmatrix} \frac{1}{2}\begin{pmatrix} t + t' e^{-ika} \\ -4V\delta_{\text{in}} - 4V'\delta_{\text{out}} e^{-ika} \end{pmatrix} & 2(V\Delta_{\text{in}} + V'\Delta_{\text{out}} e^{-ika}) \\ -2\left(V\Delta_{\text{in}} + V'\Delta_{\text{out}} e^{-ika}\right) & -\frac{1}{2}\begin{pmatrix} t + t' e^{-ika} \\ -4V\delta_{\text{in}} - 4V'\delta_{\text{out}} e^{-ika} \end{pmatrix} \end{pmatrix}. \tag{5}$$

The topological invariant v is then calculated as follows [58–60],

$$v = -Tr \int_{-\pi}^{\pi} \frac{dk}{i2\pi} F^{-1} \partial_k F = -\int_{-\pi}^{\pi} \frac{dk}{i2\pi} \partial_k \ln Z, \tag{6}$$

where

$$\begin{aligned} Z = \det F =\ & 4(V\Delta_{\text{in}} + V'\Delta_{\text{out}} e^{-ik})^2 \\ & - \tfrac{1}{4}(t - 4V\delta_{\text{in}} + t' e^{-ika} - 4V'\delta_{\text{out}} e^{-ik})^2. \end{aligned} \tag{7}$$

C. Majorana number

To determine whether a phase contains Majorana bound states (MBSs), besides analyzing the symmetry of wave functions in a finite-length system, a more reliable method is to calculate Majorana number [50,61]. The Majorana number is defined at the time-reversal-invariant momenta $k = 0$ and π. However, the Hamiltonians at $k = 0$ and π do not satisfy $h^T(k) = -h(k)$ for Pfaffian calculations. Thus, we transform

the Hamiltonians by $\eta_x \otimes \tau_0$. The Majorana number can then be calculated from

$$M = \mathrm{sgn}\{Pf[\eta_x \otimes \tau_0 h(k=0)]Pf[\eta_x \otimes \tau_0 h(k=\pi)]\} = \mathrm{sgn}\left\{\begin{matrix}\left[\frac{1}{4}(t - 4V\delta_{\mathrm{in}} + t' - 4V'\delta_{\mathrm{out}})^2 - 4(V\Delta_{\mathrm{in}} + V'\Delta_{\mathrm{out}})^2\right] \\ \left[\frac{1}{4}(t - 4V\delta_{\mathrm{in}} - t' + 4V'\delta_{\mathrm{out}})^2 - 4(V\Delta_{\mathrm{in}} - V'\Delta_{\mathrm{out}})^2\right]\end{matrix}\right\}. \quad (8)$$

D. Quantum circuit Hamiltonian and Jordan–Wigner transformation

Figure 1(b) shows a serial circuit of CPBs and JJs. Each isolated JJ connects two CPBs. In the following calculations, N is the number of CPBs, C_{gi} and V_{gi} are, respectively, the capacitance and the gate voltage of the ith CPB, C_{Ji}, V_{Ji}, and ϕ_i are, respectively, the capacitance, voltage, and phase of the JJ in the ith CPB, and $C_{Ji,i+1}$, $V_{Ji,i+1}$, and $\phi_{i,i+1}$ are, respectively, the capacitance, voltage, and phase of the isolated JJ. These parameters are also marked in Fig. 1(b). The kinetic part of the Hamiltonian of the one-dimensional system is a charging term for all capacitances:

$$E_K = \sum_{i=1}^{N}\left[\frac{1}{2}C_{Ji}V_{Ji}^2 + \frac{1}{2}C_{gi}(V_{gi} - V_{Ji})^2\right] + \sum_{i=1}^{N-1}\frac{1}{2}C_{Ji,i+1}V_{i,i+1}^2, \quad (9)$$

where $V_{Ji} = \frac{\hbar}{2e}\dot{\phi}_i$, $V_{i,i+1} = \frac{\hbar}{2e}(\dot{\phi}_i - \dot{\phi}_{i+1})$. The potential energies from the JJs are [62,63]

$$E_P = \sum_{i=1}^{N} E_{Ji}(1 - \cos\phi_i) + \sum_{i=1}^{N-1} E_{Ji,i+1}[1 - \cos(\phi_i - \phi_{i+1})], \quad (10)$$

where E_{Ji} and $E_{Ji,i+1}$ are the Josephson energies of the CPB and the isolated JJ, respectively. We then obtain the system Lagrangian $L = E_K - E_P$. We introduce $\hat{m}_i$ as the number of Cooper pairs conjugated to the superconducting phase ϕ_i.

$$\begin{pmatrix} \hat{m}_1 - m_{g1} \\ \hat{m}_2 - m_{g2} \\ \vdots \\ \hat{m}_N - m_{gN} \end{pmatrix} = \frac{\hbar}{(2e)^2}\begin{pmatrix} C_{J1} + C_{g1} + C_{J1,2} & -C_{J1,2} & 0 & \cdots \\ -C_{J1,2} & C_{J1,2} + C_{J2} + C_{g2} + C_{J2,3} & -C_{J2,3} & \vdots \\ 0 & -C_{J2,3} & \ddots & \ddots \\ \vdots & \cdots & \ddots & C_{JN-1,N} + C_{JN} + C_{gN} \end{pmatrix}\begin{pmatrix} \dot{\phi}_1 \\ \dot{\phi}_2 \\ \vdots \\ \dot{\phi}_N \end{pmatrix}, \quad (11)$$

where $m_{gi} = -\frac{C_{gi}V_{gi}}{2e}$. It may be shortened to $\mathbf{M} = \mathcal{C}\Psi$ and $\mathcal{C}$ is a N-dimensional tridiagonal matrix. For convenience we define $\dot{\phi}_i = \sum_{j=1}^{N} u_{ij}(\hat{m}_j - m_{gj})$, where u_{ij} is the matrix element of $\mathcal{C}^{-1}$. The Hamiltonian then reads

$$H = \sum_{i=1}^{N}\hbar\hat{m}_i\dot{\phi}_i - L = \sum_{i=1}^{N}\left[\frac{1}{2}\left(\frac{\hbar}{2e}\right)^2(C_{Ji} + C_{gi})\left(\sum_{j=1}^{N}u_{ij}(\hat{m}_j - m_{gj})\right)^2 - \frac{1}{2}C_{gi}V_{gi}^2\right]$$
$$+ \sum_{i=1}^{N-1}\left(\frac{\hbar}{2e}\right)^2\frac{C_{Ji,i+1}}{2}\left[\sum_{j=1}^{N}(u_{ij} - u_{i+1,j})(\hat{m}_j - m_{gj})\right]^2 + \sum_{i=1}^{N}E_{Ji}(1 - \cos\phi_i) + \sum_{i=1}^{N-1}E_{Ji,i+1}[1 - \cos(\phi_i - \phi_{i+1})]. \quad (12)$$

We ignore the constant term in the following. As per Ref. [62], the full Hamiltonian is projected onto the two charge states $|0\rangle$ and $|1\rangle$. The four terms of Eq. (12) can be rewritten as

$$H_{1+2} = \sum_{i,j=1\ (i\neq j)}^{N} Y_{ij}\sigma_i^z\sigma_j^z, \quad (13)$$

$$H_3 = -\sum_{i=1}^{N} E_{Ji}\sigma_i^x, \quad (14)$$

$$H_4 = -\sum_{i=1}^{N-1}\frac{E_{Ji,i+1}}{2}(\sigma_i^+\sigma_{i+1}^- + \sigma_i^-\sigma_{i+1}^+), \quad (15)$$

where the first two terms of Eq. (12) are merged into H_{1+2}, the third and fourth terms correspond to H_3 and H_4, respectively, σ is the Pauli matrix, and

$$Y_{ij} = \frac{1}{4}\left(\frac{\hbar}{2e}\right)^2\sum_{l=1}^{N}\begin{bmatrix}(C_{Jl} + C_{gl})u_{li}u_{lj} + \\ C_{Jl,l+1}(u_{li} - u_{l+1,i})(u_{lj} - u_{l+1,j})\end{bmatrix}. \quad (16)$$

The total Hamiltonian in the spin representation is then given by

$$H_{\mathrm{Pauli}} = H_{1+2} + H_3 + H_4. \quad (17)$$

Furthermore, we employ the Jordan–Wigner transformation to transform the Hamiltonian [64,65]. The transformation

is $\sigma_j^+ = 2c_j^\dagger e^{i\psi_j}$ and $\sigma_j^- = 2c_j e^{-i\psi_j}$, where $c_j^\dagger$ and c_j are, respectively, creation and annihilation operators, the phase $\psi_j = \pi \sum_{l<j} \hat{n}_l$, and $\hat{n}_l = c_l^\dagger c_l$ is the occupation number of fermions. In addition, $e^{\pm i\psi_j} = e^{\pm i\pi\hat{n}_1} e^{\pm i\pi\hat{n}_2} \cdots e^{\pm i\pi\hat{n}_{j-1}} = (1-2\hat{n}_1)(1-2\hat{n}_2)\cdots(1-2\hat{n}_{j-1})$. Thus, the relations between Pauli operators and creation and annihilation operators can be further rewritten as

$$\sigma_j^+ = 2c_j^\dagger(1-2\hat{n}_1)(1-2\hat{n}_2)\cdots(1-2\hat{n}_{j-1}), \tag{18}$$

$$\sigma_j^- = 2c_j(1-2\hat{n}_1)(1-2\hat{n}_2)\cdots(1-2\hat{n}_{j-1}), \tag{19}$$

$$\begin{aligned}\sigma_j^x &= (\sigma_j^+ + \sigma_j^-)/2 \\ &= (c_j^\dagger + c_j)(1-2\hat{n}_1)(1-2\hat{n}_2)\cdots(1-2\hat{n}_{j-1}),\end{aligned} \tag{20}$$

$$\sigma_j^z = \tfrac{1}{2}\sigma_j^+\sigma_j^- - 1 = 2c_j^\dagger c_j - 1. \tag{21}$$

Substituting these equations into the Hamiltonian H_{Pauli} and simplifying it gives

$$\begin{aligned}H_{JW} = &-\sum_{i=1}^{N-1} 2E_{Ji,i+1}(c_i^\dagger c_{i+1} + c_{i+1}^\dagger c_i) \\ &+ \sum_{i,j=1\ (i\neq j)}^{N} Y_{ij}(2\hat{n}_i - 1)(2\hat{n}_j - 1) \\ &- \sum_{i=1}^{N} E_{Ji}[(c_i^\dagger + c_i)(1-2\hat{n}_1)(1-2\hat{n}_2)\cdots(1-2\hat{n}_{i-1})].\end{aligned} \tag{22}$$

The third term is a particle nonconserving term and can be made negligible by tuning E_{Ji} to a quite small value (even zero). It will be discussed in detail.

III. SELF-CONSISTENT SOLUTIONS

A. Phase diagrams

To demonstrate the ground-state physics of this interacting system, we plot the $V - V'$ phase diagram with different hopping integrals in Fig. 2. When $V = V' = 0$, the system, which corresponds to the original SSH model, can be in a topologically trivial or nontrivial phase. Finite V and V' can induce rich phase transitions. The phase diagram shows six phases, including intra- and intercell-hopping (intra- and inter-CH) phases, intra- and intercell-superconducting-pairing (Intra- and Inter-CSP) phases, a coexisting (CE) phase, and a charge-density-wave (CDW) phase. The number of corresponding zero-energy modes in a finite-length system is 0, 2, 0, 4, 2, and 0, respectively. We first focus on the case of $t = 1, t' = 2$ [Fig. 2(a)] to perform a detailed analysis.

(i) When V or V' is negative and its strength is sufficiently large, it will produce an attractive interaction between nearest-neighbor sites, leading to a superconducting phase. In this phase, all order parameters are nonzero, but the Intra- or Inter-CSP order strength ($|\Delta_{\text{in}}|$ or $|\Delta_{\text{out}}|$) is much larger than the others. To clearly exhibit the characteristics of the superconducting phase and the phase transitions, we plot in

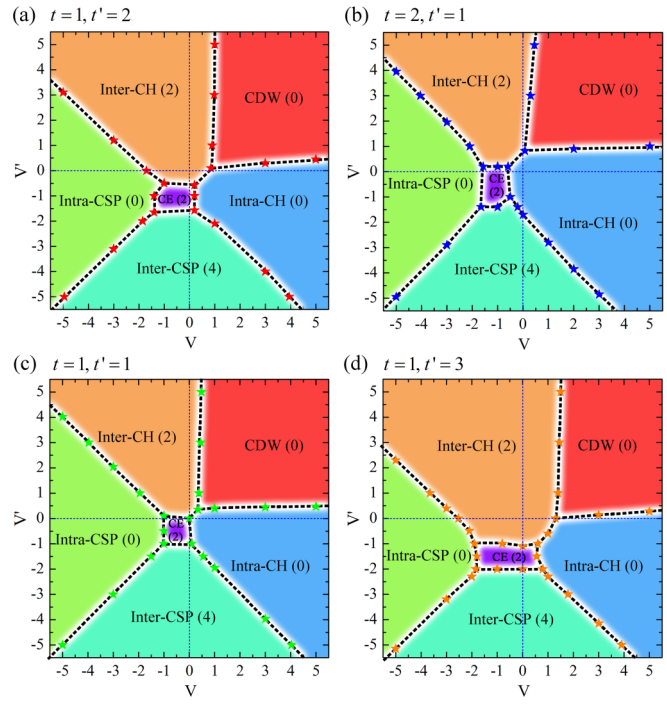

FIG. 2. Phase diagrams as functions of V and V' with (a) $t = 1, t' = 2$, (b) $t = 2, t' = 1$, (c) $t = 1, t' = 1$, and (d) $t = 1, t' = 3$. Each phase diagram consists of six phases, including intra- and intercell-hopping (Intra- and Inter-CH) phases, intra- and intercell-superconducting-pairing (Intra- and Inter-CSP) phases, a coexisting (CE) phase, and a charge-density-wave (CDW) phase. The number in parentheses gives the number of zero-energy modes in the corresponding finite-length system. The stars are the critical points that are calculated in detail. Triple points are approximated.

Fig. 3 total energy, occupation number, and order parameters as functions of V' with $V = 3$. Figs. 3(c)–3(f) show the evolution of $|\Delta_{\text{in}}|$, $|\Delta_{\text{out}}|$, $|\delta_{\text{in}}|$, $|\delta_{\text{out}}|$ in the Inter-CSP, Intra-CH, and CDW phases, respectively. When $V' < -4$, the one-dimensional system is in the Inter-CSP phase and $|\Delta_{\text{out}}|$

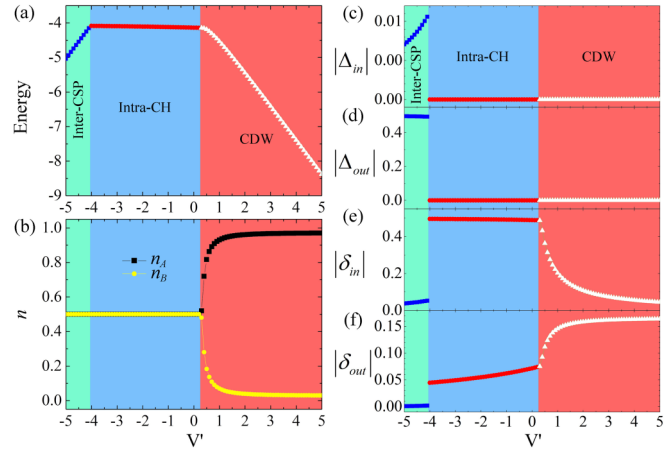

FIG. 3. For $t = 1, t' = 2, V = 3$, (a) total energy, (b) occupation number. and (c-f) order parameters as functions of V'. Green, blue, and red background colors respectively correspond to the Inter-CSP, Intra-CH, and CDW phases in Fig. 2.

is much greater than the other order parameters. In addition, since there exist intrinsic hopping terms t and t', the Intra- and Inter-CH order parameters are always nonzero in any given phase.

(ii) When V or V' is positive and sufficiently large, the corresponding superconducting pairing is completely suppressed because of the repulsive interaction between nearest-neighbor sites. From the decoupled mean-field terms in Eq. (2), we know that the minus sign in front of δ_x hopping terms favors system stability with increasing V or V'. These hopping terms also affect the intrinsic hopping terms mathematically. This can enhance the hopping integral and also induce a topological phase transition. For example, for $t = 1, t' = 2$ the system is topologically nontrivial without nearest-neighbor interactions. When V is large enough, the system enters into a topologically trivial phase without any topological edge mode at the Fermi level.

(iii) When both V and V' are sufficiently large, the repulsive interactions between nearest-neighbor sites will cause spontaneous symmetry breaking so that the occupation numbers of sublattices A and B differ [Fig. 3(b)]. This makes the system enter a CDW phase. With increasing repulsive interaction, one sublattice gradually fills and the other one empties. Meanwhile, the superconducting pairing is totally suppressed.

(iv) When both V and V' are small and negative, the system enters a CE phase, where the strengths of four order parameters ($|\Delta_{\text{in}}|$, $|\Delta_{\text{out}}|$, $|\delta_{\text{in}}|$, $|\delta_{\text{out}}|$) are comparable to each other. Fig. 4 shows energy, band gap, and order parameters as functions of V' with $V = -1$. Upon increasing V', the system goes through the Inter-CSP, CE, and Inter-CH phases. In particular, from the Inter-CSP phase to the CE phase the band gap closes and then reopens, which corresponds to a topological phase transition. The number of zero-energy modes changes from 4 to 2. Note also that all order parameters and the total energy change smoothly during this process. In Figs. 4(g)–4(i) we plot the energy levels and weight distribution of zero-energy wave functions in the CE phase, where we use a length of 100 unit cells and $V = -1$, $V' = -1$. There are two states at the Fermi level. In Fig. 4(h) the contribution from the B sublattice are totally suppressed, and the electron and hole parts of the A-sublattice components have opposite signs. The wave function satisfies $i\varphi = (i\varphi)^\dagger$ and is localized at the left end of the chain. Thus, it may be a MBS. In Fig. 4(i) the A-sublattice components are totally suppressed, and the electron and hole wave functions of the B-sublattice components are equal to each other. The corresponding wave function satisfies $\varphi = \varphi^\dagger$ and is localized at the right end of the chain. It also looks like a MBS. Naturally, the linear combinations of the two zero-energy modes also share the same characteristics.

Fig. 2(b) shows the phase diagram with $t = 2, t' = 1$. Comparing the shape of the phases between the two cases of $t = 1, t' = 2$ and $t = 2, t' = 1$ reveals an interesting phenomenon in which the two phase diagrams are symmetric about the diagonal line $V = V'$. The physical reason for this result is that the exchange of the values of t and t' leads to the exchange of the strength of intra- and intercell order parameters, so that the shape of the area in the two phase diagrams has a mirror symmetry about $V = V'$. Note that this result is based on the shape of phase areas but not on the specific phases for the symmetry.

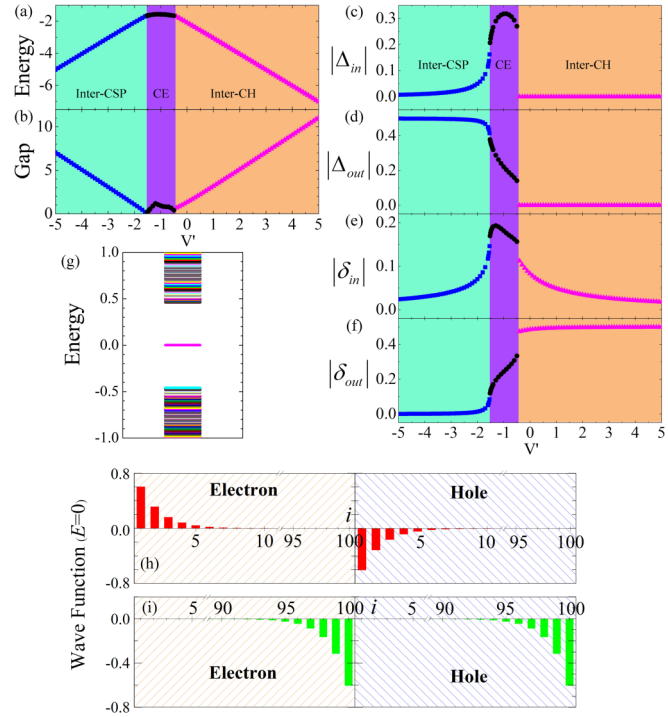

FIG. 4. For $t = 1, t' = 2, V = -1$, (a) total energy, (b) band gap, and (c-f) order parameters as functions of V'. Green, purple, and orange background colors respectively correspond to the Inter-CSP, CE, and Inter-CH phases in Fig. 2. (g) Energy levels and (h-i) spatial distribution of two zero-energy wave functions in a one-dimension system of 100 unit cells with $V' = -1$. The two wave functions are purely real. In panels (h) and (i), left and right parts correspond to electron states ($c_{iA/B}$) and hole states ($c^\dagger_{iA/B}$), respectively. Red and green bars label the components of the A and B sublattices, respectively.

To present how hopping integrals affect on the phase transitions, we plot phase diagrams for $t = 1, t' = 1$ and $t = 1, t' = 3$ in Figs. 2(c) and 2(d), respectively. Two significant changes occur with increasing t'. (i) The CE phase moves downward, which can be explained as follows. Increasing t' suggests enhanced itinerancy of particles between nearest-neighbor unit cells. In order to keep the strength of the superconducting pairing between unit cells not completely suppressed by the intercell hopping, it requires to increase the attractive interaction V', leading to the downward shift of the CE phase. (ii) The phase boundary between the Inter-CH and CDW phases moves rightward and the phase boundary between the Inter-CH and Intra-CSP phases moves downward. A direct competitive relationship exists between the Inter-CH phase and other phases. When t' is increased, it will make the size of the Inter-CH phase expanded.

B. Symmetry classification of Hamiltonians

Our self-consistent results show that the hopping order parameters δ_{in} and δ_{out} are real numbers and that the superconducting order parameters Δ_{in} and Δ_{out} have $U(1)$ symmetry. Without loss of generality, Δ_{in} and Δ_{out} are set to be real.

TABLE I. Symmetry classification of Hamiltonians of the six phases (Intra- and Inter-CH, Intra- and Inter-CSP, CE, and CDW phases) depending on the presence or absence of time-reversal symmetry (TRS), particle-hole symmetry (PHS), and sublattice symmetry (SLS). Symmetry operators are presented. $+1$, -1, and 0 in brackets are defined as per Ref. [66].

Phase	TRS	PHS	SLS	Class
Intra-/Inter-CH	K $(+1)$	$\tau_z K$ $(+1)$	τ_z (1)	BDI
Intra-/Inter-CSP, CE	$\eta_0 \otimes \tau_0 K$ $(+1)$	$\eta_x \otimes \tau_0 K$ $(+1)$	$\eta_x \otimes \tau_0$ (1)	BDI
Intra-/Inter-CH	K $(+1)$	(0)	(0)	AI

We use two sets of standard Pauli matrices (τ_μ and η_μ) and the complex-conjugation operator K to describe symmetry operations of Hamiltonians. Furthermore, $\mu = 0, x, y, z$, τ_0 and η_0 are 2×2 unit matrices, τ_μ acts on the two sublattice indices, and η_μ is used to represent the particle-hole space appearing in the Bogoliubov–de Gennes (BdG) Hamiltonian for quasiparticles in superconducting phases. The symmetry classification of the Hamiltonians of the Intra- and Inter-CH phases, Intra- and Inter-CSP phases, CE phase, and CDW phase is shown in Table I. The first five phases belong to the BDI class and the last phase belongs to the AI class [66].

C. Topological invariant and Majorana number

To verify the topological phase transitions and the existence of MBSs, we further calculate the topological invariant and the Majorana number. Since the Hamiltonians of the five phases (Intra- and Inter-CSP, Intra-and Inter-CH, and CE phases) belong to BDI class, they have an associated Z topological invariant v (winding number) [66]. The Majorana number M is calculated by following Ref. [50,61]. Details are in the Methods. When $M = -1$, there are MBSs at the ends of the one-dimensional chain. When $M = 1$, there are no MBSs. In Fig. 5 we plot v and M in two different directions ($V = -1$ and $V' = -1$), both of which cross the CE phase. All of the order parameters are determined by self-consistent calculations. For $V = -1$, upon increasing V', the system goes through three phases: the Inter-CSP phase, CE phase, and Inter-CH phase. The critical point between the Inter-CP and CE phases in Figs. 5(a) and 5(b) is in quantitative agreement with that obtained by analyzing zero-energy gap and edge states. In the two phases, there are respectively two and one edge states at each end of the one-dimensional chain. It is consistent with the topological invariant $v = 2$ and 1. However, there is also one zero-energy edge state at each end in the Inter-CH phase, which can not be distinguished from the CE phase only by the topological invariant. The Majorana number can further distinguish the two phases. The results of the calculation show that $M = -1$ only in the CE phase, which means that MBSs exist only in the CE phase, whereas the zero-energy edge states are not MBSs in the other phases. This result is consistent with our previous analysis of wave functions. For $V' = -1$ in Figs. 5(c) and 5(d), there are also three phases: the Intra-CSP phase, CE phase, and Intra-CH phase, with increasing V'. Fig. 2(b) has shown that in the Intra-CSP and Intra-CH phases there is no zero-energy state, which is consistent with the topological invariant $v = 0$.

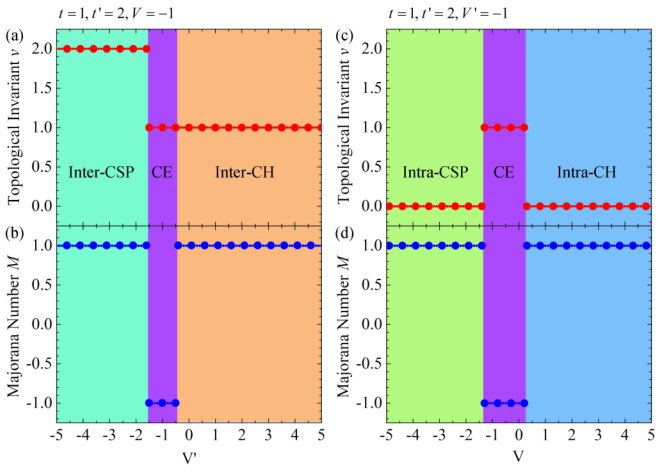

FIG. 5. For $t = 1, t' = 2$, evolution of topological invariant and Majorana number in directions $V = -1$ and $V' = -1$.

Up to now, MBSs in one-dimension systems have been widely studied [61,67–76]. Most of related researches focus on the Kitaev chain, which describes the dynamics of one-dimensional spinless fermions with superconducting p-wave pairing. One may wonder whether the interacting SSH chain at mean-field level can be reduced to the Kitaev chain for $t = t'$ and $V = V'$. The phase diagram with $t = t' = 1$ has been plotted in Fig. 2(c). We find that when the attraction ($V = V'$) is samll, the system is in the CE phase with MBSs and shows a similar topological feature as the Kitaev chain. When the attraction is sufficiently large, there is a spontaneous symmetry breaking with $|\Delta_{\text{in}}| \neq |\Delta_{\text{out}}|$, which is different from the result of the Kitaev chain. The main reason is that the SSH chain is separated into two sublattices and calculated self-consistently, while the superconducting pairing in the Kitaev model is induced by proximity of a p-wave superconductor [61].

IV. QUANTUM SIMULATION

A. Hamiltonian

Recently, the noninteracting SSH model has been successfully simulated using ^{87}Rb atoms in a momentum-space lattice [53], a resistor-inductor-capacitor (RLC) circuit [54], and a superconducting circuit [55], respectively. Especially for the last one, it is the first time to report an observation of topological insulator states through measuring a time-averaged chiral displacement in a superconducting qubit chain. For the interacting SSH model, we propose a simulation method through coupling multiple superconducting qubits and JJs, as shown in Fig. 1(b). The Hamiltonian for this quantum

circuit is derived in Sec. II D using a standard procedure. Projected on the two charge states $\{|0\rangle\ |1\rangle\}$, it is given in a spin representation,

$$H_{\text{Pauli}} = -\sum_{i=1}^{N-1} \frac{E_{Ji,i+1}}{2}(\sigma_i^+\sigma_{i+1}^- + \sigma_i^-\sigma_{i+1}^+) + \sum_{i,j=1\ (i\neq j)}^{N} Y_{ij}\sigma_i^z\sigma_j^z - \sum_{i=1}^{N} E_{Ji}\sigma_i^x, \tag{23}$$

where Y_{ij} has been defined in Eq. (16). Further use the Jordan–Wigner transformation to change the system Hamiltonian from the spin representation to a fermion representation [64,65]

$$H_{JW} = -\sum_{i=1}^{N-1} 2E_{Ji,i+1}(c_i^\dagger c_{i+1} + c_{i+1}^\dagger c_i) + \sum_{i,j=1\ (i\neq j)}^{N} Y_{ij}(2\hat{n}_i - 1)(2\hat{n}_j - 1), \tag{24}$$

where the third term of Eq. (23) has been ignored. In practice, the JJ in a CPB can be split as two parallel ones and the corresponding Josephson energy E_{Ji} can be tuned to zero by applying an external flux [19,77,78]. Nevertheless, we still investigated its effects on properties of the designed quantum circuit, and the results will be presented in the following. We theoretically determine that the third term of H_{Pauli}, as a particle nonconserving term, can be made negligible by decreasing E_{Ji} to a small value. In the first term of Eq. (24) $E_{Ji,i+1}$ is the Josephson energy of the JJ that connects nearest-neighbor CPBs; this term can correspond to the hopping term for electrons. The second term Y_{ij} contains charge energies contributed by all the capacitances; this term can be used to describe the Coulomb interaction.

The intrinsic capacitance of the JJ is close to zero [33]. Thus, C_{Ji} and $C_{Ji,i+1}$ are much less than C_{gi}, implying that Y_{ij} can change only in a very limited range. There is an effective solution to enlarge the range: Add a shunt capacitance across the JJ, as done in a transmon [20]. Since the capacitance is added in parallel with JJs, it can increase C_{Ji} and $C_{Ji,i+1}$ equivalently and make Y_{ij} change in a larger range. To show the short-range character of Y_{ij}, we consider a simple case where we set $C_{gi} = C_g$, $C_{Ji} = C_{Ji,i+1} = C_J$ and use 12 CPBs. Fig. 6(a) plots Y_{ij} as a function of i and j with $C_J/C_g = 1$. Because Y_{ii} corresponds to a constant term in the Hamiltonian, we neglect it here. One can see that Y_{ij} rapidly decays with increasing the distance between i and j, suggesting that Y_{ij} is a short-range interaction. In Fig. 6(b), Y_{1j} with different C_J/C_g also presents a short-range character. To display more intuitively the character over a large range of C_J/C_g, we plot Y_{12}, Y_{13}, and their ratio as functions of C_J/C_g in Fig. 6(c). As C_J/C_g increases, Y_{12} and Y_{13} first increase and then decrease. They peak at about $C_J/C_g = 0.5$ and 1, respectively. However, their ratio decreases monotonically. To simulate the interacting SSH model, we ignore all interactions except the nearest-neighbor one, and the nearest-neighbor interaction strength should be appropriate. Although a smaller C_J/C_g leads to a shorter-range interaction, the interaction strength will be weaker. The capacitance must be suitable to simulate

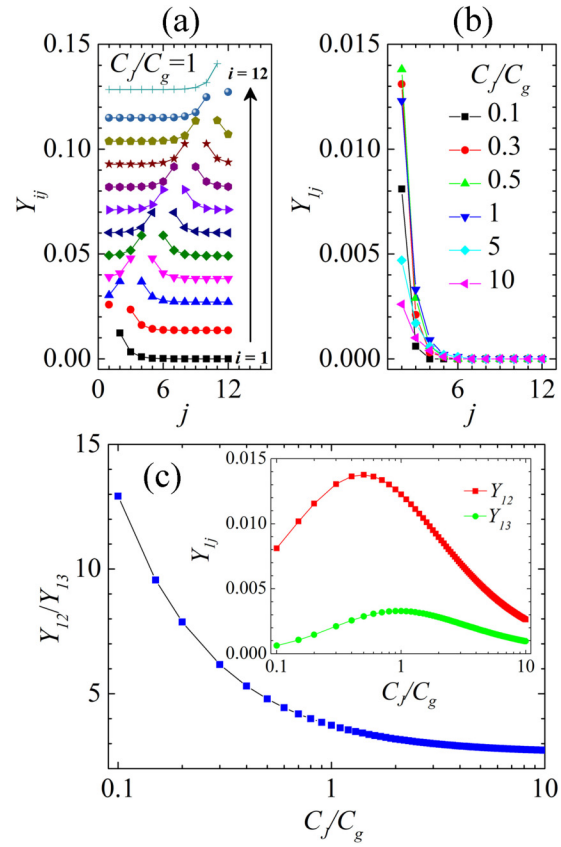

FIG. 6. A system with 12 CPBs is considered. (a) Y_{ij} as a function of i and j for $C_J/C_g = 1$. (b) Y_{1j} as a function of j with different C_J/C_g. (c) Y_{12}, Y_{13} (inset), and their ratio Y_{12}/Y_{13} as functions of C_J/C_g.

different states. By further changing the Josephson energies and the capacitances, the CPBs can be separated into A and B sublattices, then a form of the interaction SSH Hamiltonian can be obtained.

Note that the simulation of superconducting phases (including Intra-CSP, Inter-CSP, and CE phases) requires an attractive interaction, implying that Y_{ij} must be negative. From the definition of Y_{ij} [Eq. (16)], we find that it requires negative capacitances. Although Khan *et al.* detected a negative capacitance experimentally in ferroelectrics [79,80], it can not be used in a quantum circuit due to its intrinsic instability and a negative capacitance may also invalidate the projection onto the two charge states $|0\rangle$ and $|1\rangle$. Therefore, the negative-interaction part of the phase diagram in Fig. 2 is thermodynamically unstable in the current quantum circuit. But we find that several groups have investigated and realized quantum simulations of the attractive interactions. For example, the quantum simulation of the Hubbard model with attractive interactions using atoms in optical lattices has been discussed in detail by Ho *et al.* [81]; Bloch *et al.* showed quantum simulations of attractive interactions with ultracold quantum gases [82]; a proposal by Cai *et al.* suggested that nuclear spins attached to a diamond surface and addressed through nitrogen-vacancy centers could offer an attractive route toward a large-scale quantum simulator for strongly correlated systems [83]; in particular, Lu *et al.* [84] and Barends

et al. [35] could successfully simulate near-neighbor attractive interactions based on nuclear magnetic resonance (NMR) and superconducting circuit, respectively. Although our proposed quantum circuit based on superconducting qubits can not simulate the attractive interactions in practice, we still perform theoretical calculations for different interactions including attractive ones, in order to provide theoretical predictions for future quantum simulations of the interacting SSH model.

B. Numerical simulations based on 12 qubits and finite-size scalings

Since experimental operations on superconducting devices are based on the spin representation, here we perform direct numerical simulations of the spin model of the interacting SSH chain with different numbers of qubits to predict possible results of experimental measurements in different phases. However, Greiter *et al.* suggested that nontrivial states will not be topologically protected after the Jordan–Wigner transformation from the fermion representation to the spin representation [85]. Thus, our considered spin model may only be a conventional system. But what is important is that its local properties should remain unchanged, including occupation of particles, edge states, and local orders. Therefore, we can simulate the interacting SSH model by using superconducting qubits to study its local properties and further verify the mean-field results.

From Eq. (23), with considering the nearest-neighbor interaction and ignoring the particle nonconserving term the Hamiltonian can be rewritten as

$$H=\sum_{i}\begin{bmatrix}-(E_{\rm in}\sigma_{iA}^{+}\sigma_{iB}^{-}+E_{\rm out}\sigma_{iB}^{+}\sigma_{i+1,A}^{-}+{\rm H.c.})\\ +U_{\rm in}\sigma_{iA}^{z}\sigma_{iB}^{z}+U_{\rm out}\sigma_{iB}^{z}\sigma_{i+1,A}^{z}\end{bmatrix}, \tag{25}$$

where $E_{\rm in}$ ($U_{\rm in}$) and $E_{\rm out}$ ($U_{\rm out}$) correspond to intra- and intercell hopping integrals (Coulomb interactions), respectively. We consider a finite-length chain and investigate spatial distributions of particles and local order parameters for different interactions by an ED technique.

In fermion representation, we have defined three kinds of order parameters (n_α, $\delta_{\rm in/out}$, and $\Delta_{\rm in/out}$) in Sec. II A. Through employing the Jordan–Wigner transformation, we can transform them into the spin representation.

$$\begin{aligned} n_{\sigma,i,A}&=\langle\sigma_{iA}^{+}\sigma_{iA}^{-}\rangle, \quad n_{\sigma,i,B}=\langle\sigma_{iB}^{+}\sigma_{iB}^{-}\rangle,\\ \delta_{\sigma,i,\rm in}&=\langle\sigma_{iA}^{-}\sigma_{iB}^{+}\rangle, \quad \delta_{\sigma,i+,\rm out}=\langle\sigma_{iB}^{-}\sigma_{i+1,A}^{+}\rangle,\\ \Delta_{\sigma,i,\rm in}&=\langle\sigma_{iA}^{-}\sigma_{iB}^{-}\rangle, \quad \Delta_{\sigma,i+,\rm out}=\langle\sigma_{iB}^{-}\sigma_{i+1,A}^{-}\rangle, \end{aligned} \tag{26}$$

where the subscript σ represents the spin representation, i is the index of the unit cell, $i+$ corresponds to the interaction between the ith and $(i+1)$th unit cells, and *in* (*out*) corresponds to the intracell (intercell) order. In the following we use $n_{i\alpha}$ instead of $n_{\sigma,i,\alpha}$ ($\alpha=A,B$). However, the superconducting order parameter is not a good one in the ED method because the number of particles is conserved in the basis. Instead, we use the square of its operators to define new order parameters,

$$\begin{aligned} \Lambda_{\sigma,i,\rm in}&=\langle\sigma_{iA}^{+}\sigma_{iB}^{+}\sigma_{iA}^{-}\sigma_{iB}^{-}\rangle=\langle\hat{n}_{iA}\hat{n}_{iB}\rangle,\\ \Lambda_{\sigma,i+,\rm out}&=\langle\sigma_{iB}^{+}\sigma_{i+1,A}^{+}\sigma_{iB}^{-}\sigma_{i+1,A}^{-}\rangle=\langle\hat{n}_{iB}\hat{n}_{i+1,A}\rangle, \end{aligned} \tag{27}$$

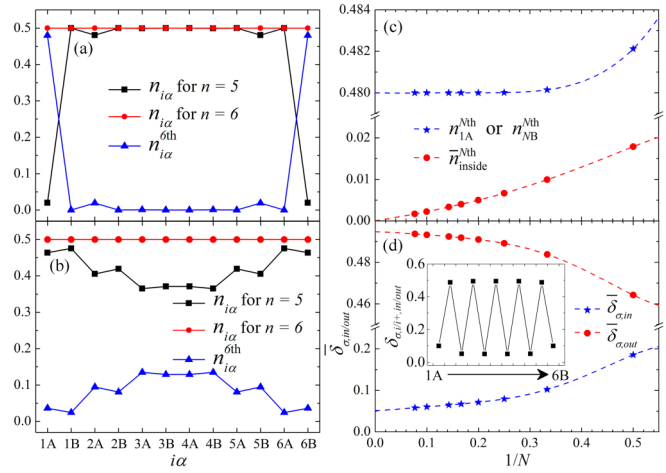

FIG. 7. Spatial distributions of particles for (a) $E_{\rm in}=1, E_{\rm out}=5$, and (b) $E_{\rm in}=5, E_{\rm out}=1$ without any nearest-neighbor interactions. The horizontal axis corresponds to 12 qubits (sites). $n_{i\alpha}^{N\rm th}=n_{i\alpha}(n=N)-n_{i\alpha}(n=N-1)$. For $E_{\rm in}=1, E_{\rm out}=5$, (c) averaged occupation numbers of the Nth added particle at edges ($n_{1A}^{N\rm th}$ or $n_{NB}^{N\rm th}$) and inside the chain ($\bar{n}_{\rm inside}^{N\rm th}$) and (d) averaged intra- and intercell hopping order parameters ($\bar{\delta}_{\sigma,\rm in}$ and $\bar{\delta}_{\sigma,\rm out}$) as functions of system size N. Dashed lines are polynomial fits for $1/N$. $\bar{n}_{\rm inside}^{j\rm th}=\frac{1}{2N-2}\sum_{i\alpha\neq 1A,NB}n_{i\alpha}^{j\rm th}$. Inset of (d): Site-resolved hopping order parameters in the chain with $N=6$.

named as intra- and intercell pairing order parameters, respectively. They can indirectly reflect the superconducting pairing.

In addition, we define an averaged hopping order parameter as

$$\bar{\delta}_{\sigma,\rm in/out}=\frac{1}{N_{\rm deg}N_{\rm in/out}}\sum_{j=1\sim N_{deg}}\sum_{i=1\sim N_{\rm in/out}}\delta_{\sigma,i/i+,\rm in/out}\Big|_{j}, \tag{28}$$

and an averaged pairing order parameter as

$$\bar{\Lambda}_{\sigma,\rm in/out}=\frac{1}{N_{\rm deg}N_{\rm in/out}}\sum_{j=1\sim N_{\rm deg}}\sum_{i=1\sim N_{\rm in/out}}\Lambda_{\sigma,i/i+,\rm in/out}\Big|_{j}. \tag{29}$$

$N_{\rm in}$ and $N_{\rm out}$ are the numbers of intra- and intercell interactions in the one-dimensional SSH chain, respectively. $N_{\rm deg}$ is the degree of degeneracy of ground states. $\bar{\delta}_{\sigma,\rm in/out}$ and $\bar{\Lambda}_{\sigma,\rm in/out}$ will be two main parameters to show finite-size scaling behavior and to reflect the effects of E_{Ji} term in our following study.

We first study the noninteracting SSH chain. Figures 7(a) and 7(b) show spatial distributions of particles for a total number of particles $n=5$ and 6 in a chain with $N=6$. The latter corresponds to a half-filling case. $n_{i\alpha}^{j\rm th}$ is the occupation number of the jth added particle at the site $i\alpha$ and satisfies $\sum_{i,\alpha}n_{i\alpha}^{j\rm th}=1$. It can be obtained through calculating the difference of occupation number between the cases of $n=j-1$ and j. When $E_{\rm in}=5$ and $E_{\rm out}=1$, the sixth added particle $n_{i\alpha}^{6\rm th}$ mainly distributes inside the chain. When $E_{\rm in}=1$ and $E_{\rm out}=5$, it distributes at the ends and shows a characteristic of edge states. This numerical result is in agreement with that obtained from the original SSH model in the fermion representation [44,45]. We can understand this method from the aspect of single-particle energy levels (bands). For the case of $N=6$ and $n=5$, when we add a new particle into

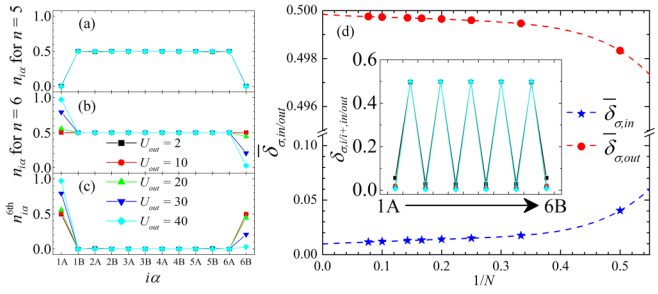

FIG. 8. Spatial distributions of particles with different intercell repulsive interactions U_{out}: $n_{i\alpha}$ for (a) $n = 5$ and (b) $n = 6$, and (c) $n_{i\alpha}^{6\text{th}}$. In (b) one of two degenerate ground states is considered, and the spatial distribution of the other ground state is opposite to that in (b) (The same applies to following figures.). (d) Averaged intra- and intercell hopping order parameters ($\overline{\delta}_{\sigma,\text{in}}$ and $\overline{\delta}_{\sigma,\text{out}}$) as functions of the system size N with $U_{\text{out}} = 10$. Inset of (d): Site-resolved hopping order parameters with different U_{out}. The intracell interaction $U_{\text{in}} = 0$.

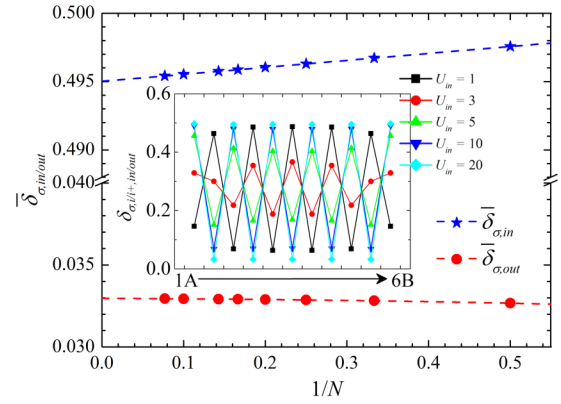

FIG. 9. Averaged intra- and interhopping order parameters ($\overline{\delta}_{\sigma,\text{in}}$ and $\overline{\delta}_{\sigma,\text{out}}$) as functions of the system size N with $U_{\text{in}} = 20$ and $U_{\text{out}} = 0$. Inset: Site-resolved hopping order parameters with different intracell repulsive interactions U_{in}.

the system, the particle must be at the highest occupied level. When $|E_{\text{out}}| > |E_{\text{in}}|$, it corresponds to the topological zero-energy edge state obtained in the fermionic model.

Furthermore, we perform a finite-size scaling to the numerical simulation. Figure 7(c) shows the occupation number at one of two ends of the SSH chain and the averaged occupation number inside the chain as functions of $1/N$ with $E_{\text{in}} = 1$ and $E_{\text{out}} = 5$. When the number of unit cell N tends to infinity ($1/N \to 0$), the occupation number at the end of the chain is stable at 0.48 and the averaged occupation number inside the chain tends to 0. A reasonable explanation can be given for the latter. Actually, when $N = 4$ the occupation number at the end has been around 0.48 (it is 0.96 at two ends in total), leading to only 0.04 particles inside the SSH chain. As the size increases, the number of inner sites becomes larger, resulting in a smaller averaged occupation number at each inner site, $0.04/(2N - 2)$. When $N \to +\infty$, the averaged occupation number will inevitably tend to 0. In Fig. 7(d), we plot finite-size scalings of the averaged hopping order parameters $\overline{\delta}_{\sigma,\text{in/out}}$ and the site-resolved hopping order parameters $\delta_{\sigma,i/i+,\text{in/out}}$ for $N = 6$. One can see that $\overline{\delta}_{\sigma,\text{out}} \gg \overline{\delta}_{\sigma,\text{in}}$ and $\delta_{\sigma,i+,\text{out}} \gg \delta_{\sigma,i,\text{in}}$. It is because the intercell hopping integral is larger than the intracell one ($E_{\text{out}} = 5E_{\text{in}}$). In addition, when $1/N < 0.2$, $n_{i\alpha}^{j\text{th}}$, $\overline{\delta}_{\sigma,\text{in}}$, and $\overline{\delta}_{\sigma,\text{out}}$ change slightly with increasing N, meaning that $N = 6$ is sufficiently large for the current ED study. We also note that, although we perform a polynomial fit for $1/N$, the scaling shows a nearly linear behavior when $1/N < 0.2$. The same behavior has also been observed in the following scaling studies.

We further investigate the cases of nonzero Coulomb interaction. In the following calculations, we set $N = 6$, $n = 6$, $E_{\text{in}} = 1$, and $E_{\text{out}} = 5$ unless stated otherwise and choose some specific interactions to show features of different phases more obviously. For example, one of the two interactions is set to be zero or $U_{\text{in}} = U_{\text{out}}$. Figures 8(a)–8(c) show spatial distributions of particles for $U_{\text{in}} = 0$ and $U_{\text{out}} = 2, 10, 20, 30, 40$. When $n = 5$, the spatial distribution is independent of U_{out} and there are 0.5 particles per site (half filling) at the middle ten sites. When $n = 6$, the occupation number only at the ends of the chain changes for different U_{out} and the distribution at the middle ten sites remain unchanged. It causes that the sixth added particle distributes at the ends of the chain and shows an edge-state characteristic. Besides, in the inset of Fig. 8(d) we can see that the intracell hopping order parameter is gradually suppressed with increasing U_{out}, while the intercell one remains at about 0.5. It is because when $U_{\text{in}} = U_{\text{out}} = 0$, $E_{\text{out}} = 5E_{\text{in}}$ has lead to the result of $\delta_{\sigma,i+,\text{out}} \gg \delta_{\sigma,i,\text{in}}$ and made $\delta_{\sigma,i+,\text{out}}$ nearly reach a maximum, so that the increasing U_{out} can not obviously raise $\delta_{\sigma,i+,\text{out}}$. Figure 8(d) shows finite size scalings of the averaged hopping order parameters $\overline{\delta}_{\sigma,\text{in/out}}$ with $U_{\text{in}} = 0$ and $U_{\text{out}} = 10$. With the increase of N, the averaged intercell hopping order parameter tends to 0.4998, and the intracell one remains a small value. We compare the results of edge states and hopping order parameters with our mean-field results. (Although their intercell hopping integrals are different, we can perform a qualitative comparison.) They can correspond to the inter-CH phase very well.

In a similar way, the case of $U_{\text{in}} > 0$ and $U_{\text{out}} = 0$ is investigated. We find that the spatial distributions of particles do not present any edge-state characteristic. In the inset of Fig. 9, we plot hopping order parameters with different intracell repulsive interactions U_{in}. With the increase of U_{in}, $\delta_{\sigma,i,\text{in}}$ is gradually enhanced and $\delta_{\sigma,i,\text{out}}$ is suppressed. For sufficiently large U_{in}, the result is similar to that of the intra-CH phase in the mean-field phase diagram. In addition, Fig. 9 shows finite size scalings of the averaged hopping order parameters $\overline{\delta}_{\sigma,\text{in/out}}$ for $U_{\text{in}} = 20$. With increasing N, $\overline{\delta}_{\sigma,\text{in}}$ and $\overline{\delta}_{\sigma,\text{out}}$ tend to 0.495 and 0.033, respectively, determining that the system is in the intra-CH phase.

For the case of $U_{\text{in}} = 0$ and $U_{\text{out}} < 0$, our calculations show that the spatial distribution of the sixth added particle cannot be obtained. It is because when the sixth particle is added the attractive interaction will change the spatial distributions of the other particles, leading to their rearrangement. But we find an obvious feature of intercell pairing with strong intercell attractive interaction in the half-filled case, as shown in Fig. 10(a). In order to further confirm the feature, we calculated hopping and pairing order parameters. The former are gradually suppressed with increasing strength of the intercell

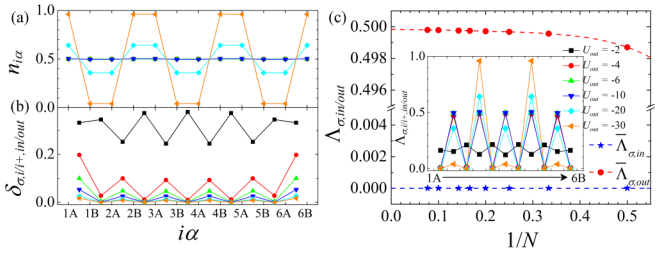

FIG. 10. (a) Spatial distributions of particles, (b) hopping order parameters, and [inset of (c)] pairing order parameters with $U_{\text{in}} = 0$ and different intercell attractive interactions U_{out}. (c) Averaged intra- and intercell pairing order parameters ($\overline{\Lambda}_{\sigma,\text{in}}$ and $\overline{\Lambda}_{\sigma,\text{out}}$) as functions of the system size N with $U_{\text{out}} = -20$.

attractive interaction, as plotted in Fig. 10(b). For the latter, we find an interesting phenomenon. In the inset of Fig. 10(c) the $2m$th intercell pairing order parameter increases with the U_{out} strength, while the $(2m-1)$th one first increases, reaches a maximum at around $U_{\text{out}} = -10$, and then decreases to zero. This behavior is totally different from the spatial distribution of particles. From the definition of the intracell pairing order parameter $\Lambda_{\sigma,i,\text{in}} = \langle \hat{n}_{iA}\hat{n}_{iB}\rangle$ (rather than $\langle \hat{n}_{iA}\rangle\langle \hat{n}_{iB}\rangle$), we think this anomalous behavior may be caused by the intrinsic quantum correlation. Next, we perform finite-size scalings of the pairing order parameters with $U_{\text{out}} = -20$ in Fig. 10(c). With the increase of size, the intracell pairing order parameter is almost 0, while the intercell one tends to 0.5, corresponding to the inter-CSP phase in the mean-field phase diagram.

Similarly, for the case of $U_{\text{in}} < 0$ and $U_{\text{out}} = 0$, spatial distributions of particles and pairing order parameters show a feature of intracell superconducting pairing and the hopping order parameters are suppressed with increasing the strength of the intracell attraction interaction U_{in} [Figs. 11(a)–11(c)], corresponding to the mean-field intra-CSP phase. Figure 11(d) shows finite-size scales of averaged pairing parameters with

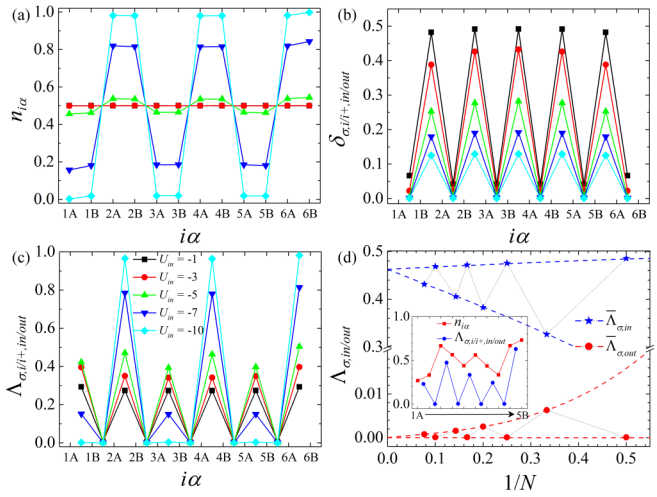

FIG. 11. (a) Spatial distributions of particles, (b) hopping order parameters, and (c) pairing order parameters with different intracell attractive interactions U_{in} and $U_{\text{out}} = 0$. (d) Averaged intra- and intercell pairing order parameters ($\overline{\Lambda}_{\sigma,\text{in}}$ and $\overline{\Lambda}_{\sigma,\text{out}}$) as functions of the system size N with $U_{\text{in}} = -7$.

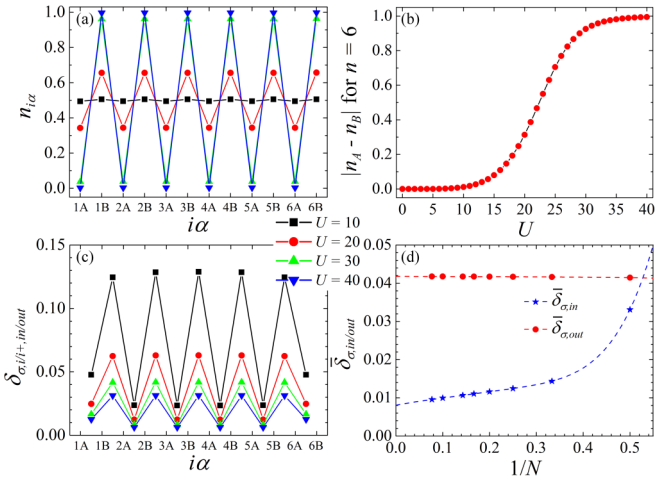

FIG. 12. (a) Spatial distributions of particles and (c) hopping order parameters with different intracell and intercell repulsive interactions and $U_{\text{in}} = U_{\text{out}} = U$. (b) The difference of particles on A and B sublattices $|n_A - n_B|$ as a function of U. (d) Averaged intra- and intercell hopping order parameters ($\overline{\delta}_{\sigma,\text{in}}$ and $\overline{\delta}_{\sigma,\text{out}}$) as functions of the system size N with $U = 30$.

$U_{\text{in}} = -7$ and $U_{\text{out}} = 0$. There exists another interesting phenomenon that the results of odd unit cells and even unit cells are completely different. They have different scaling behaviors. Through analyzing spatial distributions and pairing of particles with different sizes, we find that this phenomenon can be attributed to the different lattice symmetries (The inversion center of the former is inside the unit cell, while that of the latter is between the unit cells.) and different global pairing symmetries. For the global pairing symmetries, we give a detailed explanation below. From Fig. 11(a), we can see an obvious feature of intracell pairing with strong intracell attractive interactions for $N = 6$. However, when $N = 5$, it is not simple to remove the particles at $6A$ and $6B$ and the two sites, otherwise it will lead to a deviation from half filling. Actually, in the chain with odd unit cells particle occupation shows a seemingly irregular spatial distribution, giving rise to asymmetric pairing order parameters, as plotted in the inset of Fig. 11(d). Thus, the systems with odd and even unit cells have different global pairing symmetries. In Fig. 11(d) one can also find that in the two cases (odd and even unit cells) the trends of the pairing order parameters seem to be consistent for $N \to +\infty$, but the slope of the former is larger than that of the latter, leading to the fact that the calculation result of even unit cells is closer to that of an infinite system than that of odd unit cells. Hence, six unit cells are appropriate and sufficient to simulate properties of the one-dimensional system. When $N \to +\infty$, the averaged intracell pairing order parameter tends to $\sim$0.46 and the averaged intercell pairing order parameter tends to 0. Besides, it is worth mentioning that there do not exist such scaling behaviors in the case of the inter-CPS phase. It can be attributed to different pairing channels between the two phases.

Figures 12(a) and 12(b) show spatial distributions of particles and the difference of occupation number at A and B sublattices as a function of nearest-neighbor interactions for $U_{\text{in}} = U_{\text{out}} > 0$, respectively. We find that with increasing the

interactions, one sublattice gradually empties and the other sublattice fills, leading to a CDW order. At the same time, the hopping order parameters are gradually suppressed, as plotted in Fig. 12(c). Finite-size scalings of $\overline{\delta}_{\sigma,\text{in/out}}$ with $U_{\text{in}} = U_{\text{out}} = 30$ are shown in Fig. 12(d). We can see that the result of $N = 6$ is very close to that of an infinite system. In addition, Sirker *et al.* have also studied this interacting SSH model with only repulsive interactions using ED, Arnoldi algorithms, and light cone renormalization group [51]. Their results of fidelity susceptibility and entanglement spectra show that for sufficiently large nearest-neighbor repulsion the system is forced into the CDW state, which is in qualitative agreement with our result.

Although Greiter *et al.* suggested that nontrivial states may not be topologically protected in a spin model [85], which can be transformed into a fermion representation via the Jordan–Wigner transformation, local properties in the two representations remain unchanged. Our numerical ED results show a qualitative agreement with the above mean-field results through comparing their local properties, such as edge states, pairing states, and spatial distributions of particles. These local properties, as important features of topologically trivial or nontrivial phases, can be detected experimentally.

C. Effects of the nonconserving term

Although we have pointed out that for the particle nonconserving term the Josephson energy E_{Ji} can be tuned to zero by applying an external magnetic flux, one may wonder whether its effects are still small when E_{Ji} is a small value. For example, in fluxonium inductive energy is the smallest of the fluxonium energies, but it has a nonperturbative influence on the full energy spectrum, which presents strongly anharmonic transitions [86]. So it is necessary to investigate the effects of the particle nonconserving term on properties of our designed quantum circuit. We introduce the nonconserving term $-E_{Ji}\sigma_i^x$ back to the total Hamiltonian, which can be rewritten as

$$H = \sum_i \begin{bmatrix} -(E_{\text{in}}\sigma_{iA}^{+}\sigma_{iB}^{-} + E_{\text{out}}\sigma_{iB}^{+}\sigma_{i+1,A}^{-} + \text{H.c.}) \\ +U_{\text{in}}\sigma_{iA}^{z}\sigma_{iB}^{z} + U_{\text{out}}\sigma_{iB}^{z}\sigma_{i+1,A}^{z} - E_{Ji}\sigma_i^x \end{bmatrix}. \quad (30)$$

In the above calculations the corresponding Hilbert space is limited to the half-filling case, while in the current condition the Hilbert space has to be extended through considering different occupation number due to the fact that the number of particles are not conserved any more. The standard basis can be expressed as $|n_1 n_2 n_3 \cdots n_i \cdots n_N\rangle$ (from $|000\cdots0\cdots0\rangle$ to $|111\cdots1\cdots1\rangle$). For convenience, we assume that the Josephson energies of all qubits are equal to each other ($E_{Ji} = E_J$) and that E_J is smaller than $E_{\text{in/out}}$. For the case of $E_{\text{in}} = 1$ and $E_{\text{out}} = 5$, the range of E_J is limited to $0 \sim 1$.

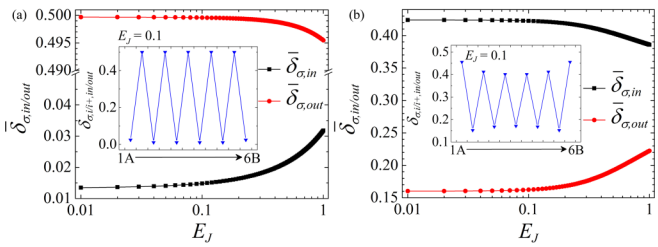

FIG. 13. Averaged hopping order parameters $\overline{\delta}_{\sigma,\text{in/out}}$ as functions of E_J with (a) $U_{\text{in}} = 0, U_{\text{out}} = 10$ and (b) $U_{\text{in}} = 5, U_{\text{out}} = 0$. Insets of (a) and (b): site-resolved hopping order parameters $\delta_{\sigma,i/i+,\text{in/out}}$ for $E_J = 0.1$.

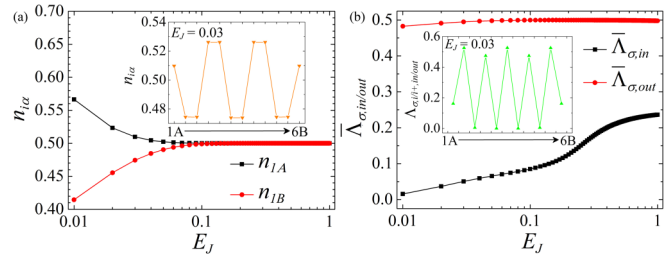

FIG. 14. (a) Occupation numbers n_{1A}, n_{1B} and (b) averaged pairing order parameters $\overline{\Lambda}_{\sigma,\text{in/out}}$ as functions of E_J with $U_{\text{in}} = 0$ and $U_{\text{out}} = -20$. Spatial distribution of particles $n_{i\alpha}$ and site-resolved pairing order parameters $\delta_{\sigma,i/i+,\text{in/out}}$ for $E_J = 0.03$ are plotted in the insets of (a) and (b), respectively.

We first investigate the case of $U_{\text{in}} = 0, U_{\text{out}} > 0$. For $E_J = 0$, our results have shown the occupation number at edges deviating from half filling and an edge-state characteristic, as shown in Fig. 8. Once $E_J > 0$ (even a small value), each site becomes half filled. This phenomenon can be attributed to enhanced quantum fluctuation of the particle occupation caused by the nonconserving term. Although the spatial distribution of particles is changed, we find that the hopping order parameters is barely affected. For instance, Fig. 13(a) shows the averaged hopping order parameters $\overline{\delta}_{\sigma,\text{in/out}}$ as functions of E_J with $U_{\text{out}} = 10$. This means that E_J cannot lead to a quantum phase transition at least in the considered range. In the inset of Fig. 13(a), we can see that the intercell hopping parameters are much larger than the intracell ones, suggesting that the system is still in the inter-CH phase. For the case of $U_{\text{in}} > 0, U_{\text{out}} = 0$, we find that E_J does not change the spatial distribution of particles and each site remains half filled. But with increasing E_J the intracell hopping order parameter decreases and the intercell one increases, as shown in Fig. 13(b) ($U_{\text{in}} = 5, U_{\text{out}} = 0$). Although a sufficiently large E_J may lead to a quantum phase transition, for a small E_J the system remains in the intra-CH phase. For example, when $E_J = 0.1$, the intracell hopping parameter $\delta_{\sigma,i,\text{in}}$ is much larger than the intercell one $\delta_{\sigma,i+,\text{out}}$.

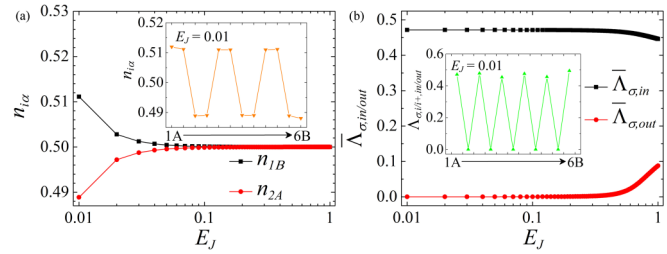

FIG. 15. (a) Occupation numbers n_{1B}, n_{2A} and (b) averaged pairing order parameters $\overline{\Lambda}_{\sigma,\text{in/out}}$ as functions of E_J with $U_{\text{in}} = -7$ and $U_{\text{out}} = 0$. Spatial distribution of particles $n_{i\alpha}$ and site-resolved pairing order parameters $\delta_{\sigma,i/i+,\text{in/out}}$ for $E_J = 0.01$ are plotted in the insets of (a) and (b), respectively.

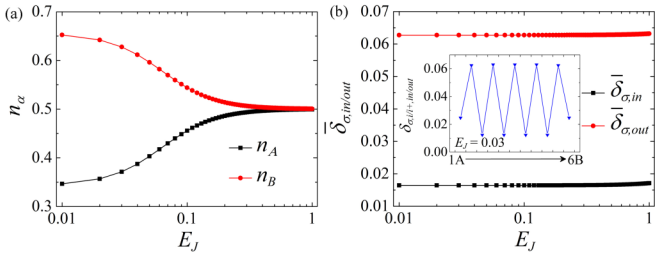

FIG. 16. (a) Occupation numbers at A and B sublattices and (b) averaged hopping order parameters $\overline{\delta}_{\sigma,\mathrm{in/out}}$ as functions of E_J with $U_{\mathrm{in}} = U_{\mathrm{out}} = 20$. Inset of (b): site-resolved hopping order parameters $\delta_{\sigma,i/i+,\mathrm{in/out}}$ for $E_J = 0.03$.

Figure 14 shows the calculation results of $U_{\mathrm{in}} = 0$ and $U_{\mathrm{out}} = -20$. We find that with the increase of E_J the occupation number at different sites gradually tends to 0.5. For example, we plot the occupation numbers at the two sites at the left end of the chain ($1A$ and $1B$) as functions of E_J in Fig. 14(a). One can see that both of them are stabilized at 0.5 with sufficiently large E_J. At the same time, the averaged intercell pairing order parameter $\overline{\Lambda}_{\sigma,\mathrm{out}}$ nearly reaches a saturation value [Fig. 14(b)], while the intracell one $\overline{\Lambda}_{\sigma,\mathrm{in}}$ and averaged hopping order parameters $\overline{\delta}_{\sigma,\mathrm{in/out}}$ are very small. It indicates that the increasing E_J does not cause a phase transition and the system is still in the inter-CSP phase. Figure 15 shows the calculation results of $U_{\mathrm{in}} = -7, U_{\mathrm{out}} = 0$. Similar to the case of the inter-CSP phase, the occupation number at each site rapidly tends to 0.5 with the increase of E_J. $\overline{\delta}_{\sigma,\mathrm{in/out}}$ and $\overline{\Lambda}_{\sigma,\mathrm{out}}$ are much lower than $\overline{\Lambda}_{\sigma,\mathrm{in}}$, meaning that E_J does not destroy the intra-CSP phase in the considered range.

Figure 16 shows the results of $U_{\mathrm{in}} = U_{\mathrm{out}} = 20$, which correspond to the CDW phase in the mean-field phase diagram. With increasing E_J, the occupation numbers at A and B sublattices gradually tend to 0.5. Meanwhile, hopping order parameters $\overline{\delta}_{\sigma,\mathrm{in/out}}$ remain small. When E_J is sufficiently large, the one-dimensional chain will be transformed into a normal insulator phase from the CDW phase.

According to the above calculation results about the effects of E_J, we can see that the introduction of the nonconserving term indeed changes properties of the interacting SSH chain. But when E_J is small (e.g., $E_J < 0.1E_{J,\mathrm{in}}$), its effects are also small so that the system can be qualitatively unchanged. Meanwhile, we also find that increasing the strength of interactions can reduce the effects of E_J. Therefore, this term can be made negligible by tuning E_J to a small value.

V. SUMMARY

In summary, we have explored topological phase transitions of the interacting SSH model with nearest-neighbor interactions and presented a rich ground-state phase diagram, where MBSs are confirmed by analyzing wave functions and Majorana number. A quantum simulation based on this model has also been proposed by connecting CPBs and JJs alternately in series. Although the proposed quantum circuit cannot simulate attractive interactions in practice, we hope that our theoretical calculations could provide useful information for future quantum simulations of the interacting SSH model.

ACKNOWLEDGMENTS

This work is supported by National Natural Science Foundation of China (Grants No. 11674152, No. U1801661, and No. 11604142), Guangdong Innovative and Entrepreneurial Research Team Program (No. 2016ZT06D348) and Natural Science Foundation of Guangdong Province (Grant No. 2017B030308003), Science, Technology and Innovation Commission of Shenzhen Municipality (Grants No. ZDSYS20170303165926217, No. JCYJ20170412152620376, and No. KYTDPT20181011104202253) and the startup funding of the Southern University of Science and Technology and the Shenzhen Peacock Plan.

[1] M. Z. Hasan and C. L. Kane, Rev. Mod. Phys. **82**, 3045 (2010).
[2] X. L. Qi and S. C. Zhang, Rev. Mod. Phys. **83**, 1057 (2011).
[3] Y. Ren, Z. Qiao, and Q. Niu, Rep. Prog. Phys. **79**, 066501 (2016).
[4] M. A. Nielsen and I. L. Chuang, *Quantum Computation and Quantum Information* (Cambridge University Press, Cambridge, 2000).
[5] J. I. Cirac and P. Zoller, Nat. Phys. **8**, 264 (2012).
[6] G. S. Paraoanu, J. Low Temp. Phys. **175**, 633 (2014).
[7] M. H. Devoret and R. J. Schoelkopf, Science **339**, 1169 (2013).
[8] F. Yang, L. Miao, Z. F. Wang, M.-Y. Yao, F. Zhu, Y. R. Song, M.-X. Wang, J.-P. Xu, A. V. Fedorov, Z. Sun, G. B. Zhang, C. Liu, F. Liu, D. Qian, C. L. Gao, and J.-F. Jia, Phys. Rev. Lett. **109**, 016801 (2012).
[9] M. König, S. Wiedmann, C. Brüne, A. Roth, H. Buhmann, L. W. Molenkamp, X.-L. Qi, and S.-C. Zhang, Science **318**, 766 (2007).
[10] L. Du, I. Knez, G. Sullivan, and R.-R. Du, Phys. Rev. Lett. **114**, 096802 (2015).
[11] C.-Z. Chang, J. Zhang, X. Feng, J. Shen, Z. Zhang, M. Guo, K. Li, Y. Ou, P. Wei, L.-L. Wang, Z.-Q. Ji, Y. Feng, S. Ji, X. Chen, J. Jia, X. Dai, Z. Fang, S.-C. Zhang, K. He, Y. Wang, L. Lu, X.-C. Ma, and Q.-K. Xue, Science **340**, 167 (2013).
[12] B. Q. Lv, H. M. Weng, B. B. Fu, X. P. Wang, H. Miao, J. Ma, P. Richard, X. C. Huang, L. X. Zhao, G. F. Chen, Z. Fang, X. Dai, T. Qian, and H. Ding, Phys. Rev. X **5**, 031013 (2015).
[13] S.-Y. Xu, I. Belopolski, N. Alidoust, M. Neupane, G. Bian, C. Zhang, R. Sankar, G. Chang, Z. Yuan, C.-C. Lee, S.-M. Huang, H. Zheng, J. Ma, D. S. Sanchez, B. Wang, A. Bansil, F. Chou, P. P. Shibayev, H. Lin, S. Jia, and M. Z. Hasan, Science **349**, 613 (2015).
[14] Z. K. Liu, L. X. Yang, Y. Sun, T. Zhang, H. Peng, H. F. Yang, C. Chen, Y. Zhang, Y. F. Guo, D. Prabhakaran, M. Schmidt, Z. Hussain, S.-K. Mo, C. Felser, B. Yan, and Y. L. Chen, Nat. Mater. **15**, 27 (2016).

[15] S.-Y. Xu, N. Alidoust, I. Belopolski, Z. Yuan, G. Bian, T.-R. Chang, H. Zheng, V. N. Strocov, D. S. Sanchez, G. Chang, C. Zhang, D. Mou, Y. Wu, L. Huang, C.-C. Lee, S.-M. Huang, B. Wang, A. Bansil, H.-T. Jeng, T. Neupert, A. Kaminski, H. Lin, S. Jia, and M. Zahid Hasan, Nat. Phys. **11**, 748 (2015).

[16] J.-P. Xu, M.-X. Wang, Z. L. Liu, J.-F. Ge, X. Yang, C. Liu, Z. A. Xu, D. Guan, C. L. Gao, D. Qian, Y. Liu, Q.-H. Wang, F.-C. Zhang, Q.-K. Xue, and J.-F. Jia, Phys. Rev. Lett. **114**, 017001 (2015).

[17] H.-H. Sun, K.-W. Zhang, L.-H. Hu, C. Li, G.-Y. Wang, H.-Y. Ma, Z.-A. Xu, C.-L. Gao, D.-D. Guan, Y.-Y. Li, C. Liu, D. Qian, Y. Zhou, L. Fu, S.-C. Li, F.-C. Zhang, and J.-F. Jia, Phys. Rev. Lett. **116**, 257003 (2016).

[18] V. Bouchiat, D. Vion, P. Joyez, D. Esteve, and M. H. Devoret, Phys. Scr. **1998**, 165 (1998).

[19] T. Duty, D. Gunnarsson, K. Bladh, and P. Delsing, Phys. Rev. B **69**, 140503(R) (2004).

[20] J. Koch, T. M. Yu, J. Gambetta, A. A. Houck, D. I. Schuster, J. Majer, A. Blais, M. H. Devoret, S. M. Girvin, and R. J. Schoelkopf, Phys. Rev. A **76**, 042319 (2007).

[21] M. Neeley, M. Ansmann, R. C. Bialczak, M. Hofheinz, E. Lucero, A. D. O'Connell, D. Sank, H. Wang, J. Wenner, A. N. Cleland, M. R. Geller, and J. M. Martinis, Science **325**, 722 (2009).

[22] M. Baur, S. Filipp, R. Bianchetti, J. M. Fink, M. Göppl, L. Steffen, P. J. Leek, A. Blais, and A. Wallraff, Phys. Rev. Lett. **102**, 243602 (2009).

[23] M. A. Sillanpää, J. Li, K. Cicak, F. Altomare, J. I. Park, R. W. Simmonds, G. S. Paraoanu, and P. J. Hakonen, Phys. Rev. Lett. **103**, 193601 (2009).

[24] W. R. Kelly, Z. Dutton, J. Schlafer, B. Mookerji, T. A. Ohki, J. S. Kline, and D. P. Pappas, Phys. Rev. Lett. **104**, 163601 (2010).

[25] A. A. Abdumalikov Jr., O. Astafiev, A. M. Zagoskin, Yu. A. Pashkin, Y. Nakamura, and J. S. Tsai, Phys. Rev. Lett. **104**, 193601 (2010).

[26] J. Li, G. S. Paraoanu, K. Cicak, F. Altomare, J. I. Park, R. W. Simmonds, M. A. Sillanpää, and P. J. Hakonen, Phys. Rev. B. **84**, 104527 (2011).

[27] J. Li, G. S. Paraoanu, K. Cicak, F. Altomare, J. I. Park, R. W. Simmonds, M. A. Sillanpää, and P. J. Hakonen, Sci. Rep. **2**, 645 (2012).

[28] J. Li, M. P. Silveri, K. S. Kumar, J. M. Pirkkalainen, A. Vepsäläinen, W. C. Chien, J. Tuorila, M. A. Sillanpää, P. J. Hakonen, E. V. Thuneberg, and G. S. Paraoanu, Nat. Commun. **4**, 1420 (2013).

[29] M. D. Schroer, M. H. Kolodrubetz, W. F. Kindel, M. Sandberg, J. Gao, M. R. Vissers, D. P. Pappas, A. Polkovnikov, and K. W. Lehnert, Phys. Rev. Lett. **113**, 050402 (2014).

[30] P. Roushan, C. Neill, Y. Chen, M. Kolodrubetz, C. Quintana, N. Leung, M. Fang, R. Barends, B. Campbell, Z. Chen, B. Chiaro, A. Dunsworth, E. Jeffrey, J. Kelly, A. Megrant, J. Mutus, P. J. J. O'Malley, D. Sank, A. Vainsencher, J. Wenner *et al.*, Nature (London) **515**, 241 (2014).

[31] X. S. Tan, Y. X. Zhao, Q. Liu, G. M. Xue, H. F. Yu, Z. D. Wang, and Y. Yu, npj Quantum Mater. **2**, 60 (2017).

[32] X. Tan, D.-W. Zhang, Q. Liu, G. Xue, H.-F. Yu, Y.-Q. Zhu, H. Yan, S.-L. Zhu, and Y. Yu, Phys. Rev. Lett. **120**, 130503 (2018).

[33] G. Wendin, Rep. Prog. Phys **80**, 106001 (2017).

[34] R. Barends, L. Lamata, J. Kelly, L. Garci'a-Alvarez, A. G. Fowler, A. Megrant, E. Jeffrey, T. C. White, D. Sank, J. Y. Mutus, B. Campbell, Y. Chen, Z. Chen, B. Chiaro, A. Dunsworth, I.-C. Hoi, C. Neill, P. J. J. O'Malley, C. Quintana, P. Roushan, A. Vainsencher, J. Wenner, E. Solano, and J. M. Martinis, Nat. Commun. **6**, 7654 (2015).

[35] R. Barends, A. Shabani, L. Lamata, J. Kelly, A. Mezzacapo, U. Las Heras, R. Babbush, A. G. Fowler, B. Campbell, Y. Chen, Z. Chen, B. Chiaro, A. Dunsworth, E. Jeffrey, E. Lucero, A. Megrant, J. Y. Mutus, M. Neeley, C. Neill, P. J. J. O'Malley, C. Quintana, P. Roushan, D. Sank, A. Vainsencher, J. Wenner, T. C. White, E. Solano, H. Neven, and J. M. Martinis, Nature (London) **534**, 222 (2016).

[36] Y. P. Zhong, D. Xu, P. Wang, C. Song, Q. J. Guo, W. X. Liu, K. Xu, B. X. Xia, C. Y. Lu, S. Y. Han, J. W. Pan, and H. H. Wang, Phys. Rev. Lett. **117**, 110501 (2016).

[37] A. J. Park, E. McKay, D. Lu, and R. Laflamme, New J. Phys. **18**, 043043 (2016).

[38] C. Song, K. Xu, W. Liu, C. P. Yang, S. B. Zheng, H. Deng, Q. Xie, K. Huang, Q. Guo, L. Zhang, P. Zhang, D. Xu, D. Zheng, X. Zhu, H. Wang, Y. A. Chen, C. Y. Lu, S. Han, and J. W. Pan, Phys. Rev. Lett. **119**, 180511 (2017).

[39] P. J. J. O'Malley, R. Babbush, I. D. Kivlichan, J. Romero, J. R. McClean, R. Barends, J. Kelly, P. Roushan, A. Tranter, N. Ding, B. Campbell, Y. Chen, Z. Chen, B. Chiaro, A. Dunsworth, A. G. Fowler, E. Jeffrey, E. Lucero, A. Megrant, J. Y. Mutus, M. Neeley, C. Neill, C. Quintana, D. Sank, A. Vainsencher, J. Wenner, T. C. White, P. V. Coveney, P. J. Love, H. Neven, A. Aspuru-Guzik, and J. M. Martinis, Phys. Rev. X **6**, 031007 (2016).

[40] A. Kandala, A. Mezzacapo, K. Temme, M. Takita, J. M. Chow, and J. M. Gambetta, Nature (London) **549**, 242 (2017).

[41] R. Islam, C. Senko, W. C. Campbell, S. Korenblit, J. Smith, A. Lee, E. E. Edwards, C.-C. J. Wang, J. K. Freericks, and C. Monroe, Science **340**, 583 (2013).

[42] J. Zhang, P. W. Hess, A. Kyprianidis, P. Becker, A. Lee, J. Smith, G. Pagano, I.-D. Potirniche, A. C. Potter, A. Vishwanath, N. Y. Yao, and C. Monroe, Nature (London) **543**, 217 (2017).

[43] S. Choi, J. Choi, R. Landig, G. Kucsko, H. Zhou, J. Isoya, F. Jelezko, S. Onoda, H. Sumiya, V. Khemani, C. von Keyserlingk, N. Y. Yao, E. Demler, and M. D. Lukin, Nature (London) **543**, 221 (2017).

[44] S. Q. Shen, *Topological Insulators: Dirac Equation in Condensed Matters* (Springer, Berlin, 2012).

[45] W. P. Su, J. R. Schrieffer, and A. J. Heeger, Phys. Rev. B **22**, 2099 (1980).

[46] J. E. Hirsch, Phys. Rev. Lett. **51**, 296 (1983).

[47] J. Voit, Phys. Rev. Lett. **64**, 323 (1990).

[48] M. Rateitzak and T. Koslowski, Chem. Phys. Lett. **377**, 455 (2003).

[49] T. Miyao, J. Stat. Phys. **149**, 519 (2012).

[50] D. Sticlet, L. Seabra, F. Pollmann, and J. Cayssol, Phys. Rev. B **89**, 115430 (2014).

[51] J. Sirker, M. Maiti, N. P. Konstantinidis, and N. Sedlmayr, J. Stat. Mech.: Theory Exp. (2014) P10032.

[52] M. Weber, F. F. Assaad, and M. Hohenadler, Phys. Rev. B **91**, 245147 (2015).

[53] E. J. Meier, F. A. An, and B. Gadway, Nat. Commun. **7**, 13986 (2016).

[54] C. H. Lee, S. Imhof, C. Berger, F. Bayer, J. Brehm, L. W. Molenkamp, T. Kiessling, and R. Thomale, Commun. Phys. **1**, 39 (2018).

[55] W. Cai, J. Han, F. Mei, Y. Xu, Y. Ma, X. Li, H. Wang, Y. P. Song, Z.-Y. Xue, Z.-Q. Yin, S. Jia, and L. Sun, Phys. Rev. Lett. **123**, 080501 (2019).

[56] M. Ezawa, Phys. Rev. B **96**, 121105(R) (2017).

[57] L. Barbiero, L. Santos, and N. Goldman, Phys. Rev. B **97**, 201115(R) (2018).

[58] Y. Wang, J.-J. Miao, H.-K. Jin, and S. Chen, Phys. Rev. B **96**, 205428 (2017).

[59] R. Wakatsuki, M. Ezawa, Y. Tanaka, and N. Nagaosa, Phys. Rev. B **90**, 014505 (2014).

[60] Q.-B. Zeng, S. Chen, and R. Lü, Phys. Rev. B **94**, 125408 (2016).

[61] A. Yu Kitaev, Phys. Usp. **44**, 131 (2001).

[62] G. Wendin and V. S. Shumeiko, arXiv:cond-mat/0508729.

[63] J. Siewert, R. Fazio, G. M. Palma, and E. Sciacca, Low. Temp. Phys. **118**, 795 (2000).

[64] P. Jordan and E. Wigner, Z. Phys. **47**, 631 (1928).

[65] E. Lieb, T. Sehultz, and D. Mattis, Ann. Phys. **16**, 407 (1961).

[66] A. P. Schnyder, S. Ryu, A. Furusaki, and A. W. W. Ludwig, Phys. Rev. B **78**, 195125 (2008).

[67] S. Gangadharaiah, B. Braunecker, P. Simon, and D. Loss, Phys. Rev. Lett. **107**, 036801 (2011).

[68] E. Sela, A. Altland, and A. Rosch, Phys. Rev. B **84**, 085114 (2011).

[69] E. M. Stoudenmire, J. Alicea, O. A. Starykh, and M. P. A. Fisher, Phys. Rev. B **84**, 014503 (2011).

[70] R. M. Lutchyn and M. P. A. Fisher, Phys. Rev. B **84**, 214528 (2011).

[71] A. M. Lobos, R. M. Lutchyn, and S. DasSarma, Phys. Rev. Lett. **109**, 146403 (2012).

[72] R. Hützen, A. Zazunov, B. Braunecker, A. L. Yeyati, and R. Egger, Phys. Rev. Lett. **109**, 166403 (2012).

[73] L. Fidkowski, J. Alicea, N. H. Lindner, R. M. Lutchyn, and M. P. A. Fisher, Phys. Rev. B **85**, 245121 (2012).

[74] F. Hassler and D. Schuricht, New J. Phys. **14**, 125018 (2012).

[75] A. Manolescu, D. C. Marinescu, and T. D. Stanescu, J. Phys. Condens. Matter **26**, 172203 (2014).

[76] O. Kashuba and C. Timm, Phys. Rev. Lett. **114**, 116801 (2015).

[77] D. Vion, A. Aassime, A. Cottet, P. Joyez, H. Pothier, C. Urbina, D. Esteve, and M. H. Devoret, *New Directions in Mesoscopic Physics (towards nanoscience)* (Springer, Netherlands, 2003).

[78] Y. Nakamura, Y. Pashkin, and J. Tsai, Nature (London) **398**, 786 (1999).

[79] G. Catalan, D. Jiménez, and A. Gruverman, Nature Mater. **14**, 137 (2015).

[80] A. I. Khan, K. Chatterjee, B. Wang, S. Drapcho, L. You, C. Serrao, S. R. Bakaul, R. Ramesh, and S. Salahuddin, Nature Mater. **14**, 182 (2015).

[81] A. F. Ho, M. A. Cazalilla, and T. Giamarchi, Phys. Rev. A **79**, 033620 (2009).

[82] I. Bloch, J. Dalibard, and S. Nascimbène, Nat. Phys. **8**, 267 (2012).

[83] J.-M. Cai, A. Retzker, F. Jelezko, and M. B. Plenio, Nat. Phys. **9**, 168 (2013).

[84] Y. Lu, G. R. Feng, Y. S. Li, and G. L. Long, Sci. Bull. **60**, 241 (2015).

[85] M. Greiter, V. Schnells, and R. Thomale, Ann. Phys. **351**, 1026 (2014).

[86] V. E. Manucharyan, J. Koch, L. I. Glazman, and M. H. Devoret, Science **326**, 113 (2009).